Heliyon 10 (2024) e36559

Contents lists available at ScienceDirect

Heliyon

journal homepage: www.cell.com/heliyon

Research article

Exploring cuproptosis-related molecular clusters and immunological characterization in ischemic stroke through machine learning

Rongxing Qin [a], Xiaojun Liang [a], Yue Yang [a,b], Jiafeng Chen [a,b], Lijuan Huang [a,b], Wei Xu [a,b], Qingchun Qin [a,b], Xinyu Lai [a], Xiaoying Huang [a], Minshan Xie [a], Li Chen [a,b,*]

[a] *Department of Neurology, The First Affiliated Hospital, Guangxi Medical University, Nanning, Guangxi Zhuang Autonomous Region, 530021, China*

[b] *National Center for International Research of Biological Targeting Diagnosis and Therapy (Guangxi Key Laboratory of Biological Targeting Diagnosis and Therapy Research), Guangxi Medical University, Guangxi Zhuang Autonomous Region, Nanning, 530021, China*

ARTICLE INFO

Keywords:
Cuproptosis-related genes
Ischemic stroke
Immune infiltration
Machine learning

ABSTRACT

Objective: Ischemic stroke (IS) is a significant health concern with high disability and fatality rates despite available treatments. Immune cells and cuproptosis are associated with the onset and progression of IS. Investigating the interaction between cuproptosis-related genes (CURGs) and immune cells in IS can provide a theoretical basis for IS treatment.

Methods: We obtained IS datasets from the Gene Expression Omnibus (GEO) and employed machine learning to identify CURGs. The diagnostic efficiency of the CURGs was evaluated using receiver operating characteristic (ROC) curves. KEGG and gene set enrichment analysis (GSEA) were also conducted to identify biologically relevant pathways associated with CURGs in IS patients. Single-cell analysis was used to confirm the expression of 19 CURGs, and pathway activity calculations were performed using the AUCell package. Additionally, a risk prediction model for IS patients was developed, and core modules and hub genes related to IS were identified using weighted gene coexpression network analysis (WGCNA). We classified IS patients using a method of consensus clustering.

Results: We established a precise diagnostic model for IS. Enrichment analysis revealed major pathways, including oxidative phosphorylation, the NF-kappa B signaling pathway, the apoptosis pathway, and the Wnt signaling pathway. At the single-cell level, compared to those in non-IS samples, 19 CURGs were primarily overexpressed in the immune cells of IS samples and exhibited high activity in natural killer cell-mediated cytotoxicity, steroid hormone biosynthesis, and oxidative phosphorylation. Two clusters were obtained through consensus clustering. Notably, immune cell types including B cells, plasma cells, and resting NK cells, varied between the two clusters. Furthermore, the red module and hub genes associated with IS were uncovered. The expression patterns of CURGs varied over time.

Conclusion: This study developed a precise diagnostic model for IS by identifying CURGs and evaluating their interaction with immune cells. Enrichment analyses revealed key pathways

* Corresponding author. Department of Neurology, The First Affiliated Hospital, Guangxi Medical University, Nanning, Guangxi Zhuang Autonomous Region, 530021, China.

E-mail address: chenli@gxmu.edu.cn (L. Chen).

https://doi.org/10.1016/j.heliyon.2024.e36559
Received 12 May 2023; Received in revised form 15 August 2024; Accepted 19 August 2024
Available online 30 August 2024

involved in IS, and single-cell analysis confirmed CURG overexpression in immune cells. A risk prediction model and core modules associated with IS were also identified.

1. Introduction

Stroke is the top cause of death and disability worldwide and is the second most common cause of death. The impact of stroke on individuals, families, and communities is substantial, with significant economic and social costs [1,2]. The most prevalent type of stroke is ischemic stroke (IS), which comprises 87 % of cases [3]. The burden increased substantially (a 70.0 % increase in incident strokes, a 43.0 % increase in deaths from stroke, a 102.0 % increase in prevalent strokes, and a 143.0 % increase in disability-adjusted life years) globally [4]. The pooled annual prevalence was 1329.5 per 100,000, with an incidence of 442.1 per 100,000, a mortality rate of 154.1 per 100,000, and a case fatality rate of 35.8 % in China [5]. IS is caused by cerebral vascular congestion and a lack of blood supply to the brain, resulting in reduced oxygen delivery to brain tissue. This hypoxic environment triggers a series of pathophysiological changes that eventually lead to brain cell death and neurological dysfunction [6]. Currently, the mainstay treatments for IS involve intravenous thrombolysis and endovascular thrombectomy. Although endovascular reperfusion therapy holds the potential for improving outcomes in specific cases, the overall prognosis for IS remains challenging due to factors like a narrow treatment window, risks of hemorrhagic complications, and subsequent reperfusion-related injuries [7–9]. Furthermore, the rt-PA treatment carries a significant risk of secondary hemorrhage [10]. Therefore, there is an urgent need to identify therapeutic targets and develop effective interventions for IS patients.

Previous research has indicated that different types of cell death, such as pyroptosis, ferroptosis, and the recently discovered cuproptosis, are associated with brain damage and neuronal death in IS [11–13]. Heavy metal, excessive intake, or abnormal accumulation of copper will lead to excess copper [14]. Cuproptosis occurs when cells accumulate excess copper, leading to programmed cell death. Aggregation of lipidized proteins in mitochondria causes instability of FE-S cluster proteins, ultimately leading to cell death [15]. Several studies have suggested that copper contributes to the development of cardiovascular and cerebrovascular diseases, including stroke, ischemia-reperfusion injury, heart failure, and atherosclerosis [16–20]. Although copper concentrations are normally low in cells, this metal is necessary as a cofactor for various essential metabolic enzymes across all cell types during normal physiological processes [16,21]. Several studies have investigated the relationship between stroke incidence and copper levels. The National Health and Nutrition Examination Survey revealed a negative correlation between copper consumption and the risk of stroke [22]. However, another study suggested that high serum copper levels may increase the risk of IS [23]. Cuproptosis is believed to contribute significantly to the development of stroke [13]. Therefore, additional research is needed to fully comprehend the mechanisms linking cuproptosis and IS.

Recent research has indicated that the immune system plays a crucial role in the pathophysiology of IS. When a stroke occurs, immune cells are rapidly recruited to the affected area. Immune cells have been found to have protective effects in certain areas, such as reducing inflammatory responses and secreting growth factors [24,25]. Despite this knowledge, the relationships between cuproptosis and immune infiltration and between cuproptosis and the progression of IS remain unclear. Therefore, further studies must be conducted to explore the mechanisms that regulate IS progression.

In this study, we compared the immune characteristics of IS patients based on cuproptosis-related genes (CURGs) expression. We identified differentially expressed genes (DEGs) using limma and analyzed their functions and pathways. The time series analysis was used to assess CURG expression changes. A prediction model for cuproptosis risk was developed using machine learning. Enrichment analyses were employed to investigate the clusters' roles in IS and immunity. The single-cell analysis identified distinct expression patterns of 19 CURGs across various cell types in the brain tissues of mice with IS. This research aims to identify biomarkers for IS diagnosis and treatment by analyzing gene expression and understanding the molecular pathways implicated in IS.

2. Materials and methods

2.1. Expression datasets of the IS

We obtained expression datasets of IS from the Gene Expression Omnibus (GEO) [26]. The inclusion criteria were as follows: (i) control and case groups, (ii) microarray or bulk RNA-seq data of mRNA, (iii) samples obtained from peripheral blood samples, and (iv) *Homo sapiens*. The exclusion criteria were as follows: (i) other types of strokes including hemorrhagic stroke and transient ischemic attack (TIA); (ii) samples involving methylation profiling by array, rather than microarray or bulk RNA-seq data of mRNA; (iii) other species types, such as *Mus musculus*, etc; (iv) samples consisting of non-coding RNA such as lncRNA or miRNA. Based on the criteria outlined above, we incorporated three datasets into our analysis. The GSE58294 dataset includes 69 IS samples and 23 non-IS samples [27]. Additionally, we utilized the GSE16561 dataset, which comprises 39 IS samples and 24 non-IS samples [28]. Furthermore, our analysis involved the GSE122709 dataset, consisting of 10 IS samples and 5 non-IS samples [29] (Supplementary Materials 1).

2.2. CURGs in IS

We obtained 58 CURGs from the FerrDb database [30] and the PubMed database [31,32].

2.3. Data processing

To preprocess the GSE58294 dataset, we performed deduplication and log transformation of the expression matrix. Next, we compared the expression levels of 58 CURGs between 69 individuals with IS and 23 control subjects using a Wilcoxon test. Our analysis revealed that 30 CURGs exhibited differential expression between the two groups.

2.4. The least absolute shrinkage and selection operator (LASSO)

The LASSO regression method can improve the predictive accuracy of a statistical model [33]. We utilized LASSO regression to assess the diagnostic potential of the 30 CURGs for IS. LASSO regression was performed with the R package "glmnet" [34]. We conducted receiver operating characteristic (ROC) curves [35] to assess the model's capacity to distinguish between IS patients and non-IS patients.

2.5. Immune infiltration analysis

The analysis of immune infiltration is crucial for understanding disease progression and treatment efficacy. To this end, we used the CIBERSORT algorithm [36] and LM22 matrix to determine the proportion of 22 immune cell types present in each sample based on gene expression data. We deemed immune cell components with $P < 0.05$ accurate and considered only those samples for analysis. The immune cell proportions in each sample were normalized to a sum of one.

2.6. Weighted gene coexpression network analysis (WGCNA)

WGCNA is a bioinformatics method that describes gene associations between different samples [37]. We constructed a coexpression network using the R package "WGCNA" by clustering genes with similar expression patterns. Through this analysis, we studied the correlation of these gene modules with specific traits or phenotypes. We included genes with an adjusted *P* value of less than 0.05 and applied a suitable soft threshold (β) to construct a scale-free network. To obtain a topological overlap matrix (TOM), we transformed the gene expression similarity matrix into an adjacency matrix using β.

2.7. Time series analysis and consensus clustering

In this study, we employed the R package "Mfuzz" to examine the temporal expression patterns of several CURGs. As the expression of these genes was measured at distinct time points, we utilized the "ConsensusClusterPlus" package for consensus clustering. By applying this technique, we stratified the IS group into two clusters based on the differential expression of the CURGs.

2.8. Gene set variation analysis (GSVA) and enrichment analysis

GSVA was used to estimate the activity of gene sets across samples by calculating the enrichment score for each set [38]. GSVA is useful for identifying active pathways or processes that are differentially active between groups of samples with biological relevance. DEGs were identified with a $|\log_2 FC| > 1$ and adj. $P < 0.05$. To investigate the biological functions of the genes, GO and KEGG enrichment analyses were performed using the "clusterProfiler" package [39].

2.9. Gene set enrichment analysis (GSEA)

We conducted a gene set enrichment analysis (GSEA) using the "clusterProfiler" package. Initially, the gene expression data were utilized to partition the samples into high and low-expression groups. Subsequently, the variance in gene expression between these groups was computed. Next, a gene ranking list was generated by sorting all the genes based on their correlation with the target gene. Finally, the cumulative enrichment score was calculated to assess the enrichment of the target gene within the entire ranked list.

2.10. Single-cell analysis

The GSE174574 single-cell dataset was used to validate gene expression [40]. We utilized the Seurat package for stringent quality control and statistical analysis of the single-cell data. The CreateSeuratObject function was employed to instantiate Seurat objects, facilitating the efficient analysis of individual cells. To ensure optimal data quality, a rigorous quality control step was conducted using specific criteria, including nFeature_RNA >500 and nFeature_RNA <5000 and percent.mt < 15. The non-IS and IS datasets were subsequently merged, and batch effect correction and data normalization steps were applied.

Principal component analysis (PCA) and uniform manifold approximation and projection (UMAP) were employed to reduce the dimensionality of the integrated dataset, enabling visualization and interpretation of the cellular heterogeneity. Cell clustering was performed using the FindNeighbors and FindClusters functions. Single-cell type annotation was conducted using the SingleR package [41], with the resulting annotations used to rename the cluster labels, enhancing their interpretability. Various visualizations, including powerful UMAP plots and informative dot plots, were generated to effectively illustrate the spatial distribution and gene expression patterns among distinct cell types.

Utilizing the AUCell R package, we conducted pathway scoring for individual cells through gene set enrichment analysis. Subsequently, we calculated the area under the curve (AUC) values for the 19 selected CURGs. Gene expression rankings were then generated for each cell, allowing estimation of the proportions of highly expressed gene sets within each cell. Cells demonstrating elevated expression levels of genes within the gene set exhibited correspondingly higher AUC values.

2.11. Statistical analysis

The data from the two groups were compared using either the Wilcoxon signed-rank test or the *t*-test, and correlation coefficients were determined through Spearman analysis. All statistical analyses were performed using R, with statistical significance assessed at a threshold of $P < 0.05$.

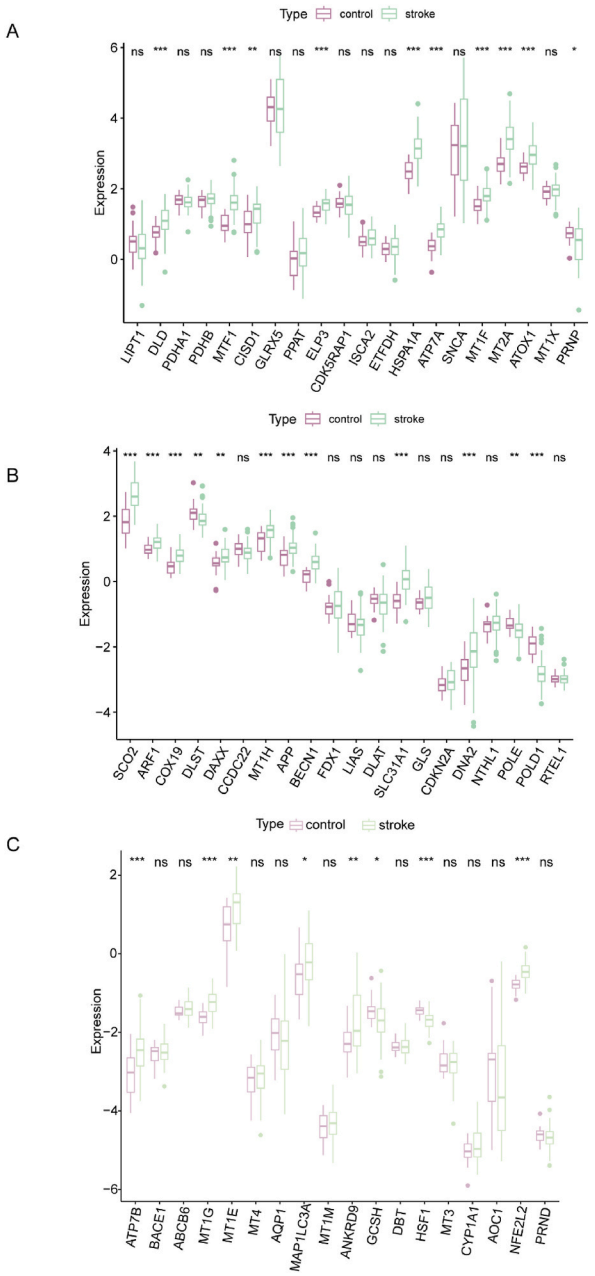

Fig. 1. Boxplots depicting the expression levels of 58 CURGs in IS and non-IS patients. (A) Boxplots of the expression levels of 20 distinct CURGs. (B) Boxplots of the expression levels of another 20 distinct CURGs. (C) Boxplots of the expression levels of 18 CURGs (*$P < 0.05$, **$P < 0.01$, ***$P < 0.001$, ****$P < 0.0001$; ns, not significant).

3. Results

3.1. The expression of CURGs in IS

Our analysis revealed that 58 CURGs showed differential expression between the IS group and the non-IS group. Specifically, the genes *DLD*, *MTF1*, *CISD1*, *ELP3*, *HSPA1A*, *ATP7A*, *MT1F*, *MT2A*, *ATOX1*, and *PRNP* were found to be significant in both the IS and non-IS groups (Fig. 1A). Similarly, *SCO2*, *ARF1*, *COX19*, *DLST*, *DAXX*, *MT1H*, *APP*, *BECN1*, *SLC31A1*, *DNA2*, *POLE*, and *POLD1* were identified as significant (Fig. 1B). Additionally, *ATP7B*, *MT1G*, *MT1E*, *MAP1LC3A*, *ANKRD9*, *GCSH*, *HSF1*, and *NFE2L2* were determined to be significant (Fig. 1C).

3.2. Lasso model construction and validation

In this study, LASSO analysis identified 19 CURGs associated with IS among the 30 CURGs analyzed (Fig. 2A–B). Heatmaps were generated to compare the expression of these 19 CURGs between the two groups (Fig. 2C–D). An AUC value of 1 suggested that these 19 CURGs have high predictability for identifying IS. ROC curves for each of the 19 CURGs were plotted, and *MTF1*, *POLD1*, and *HSPA1A* had AUC values of 0.914, 0.922, and 0.900, respectively (Fig. 2E–F). The cuproptosis-related risk scores were computed by utilizing gene expression data and their corresponding coefficients from 19 CURGs. In the Wilcoxon test, we observed that the actual median for the IS group was 1.482, while for the non-IS group, it was 0.7356, with a *P*-value of <0.0001. This indicates that the risk of cuproptosis in the IS group is significantly higher compared to the non-IS group. (Fig. 2G). The cuproptosis-related risk score was used to categorize IS patients into high and low-risk groups (Fig. 2H).

3.3. Protein-protein interaction (PPI) analysis

We analyzed the PPI network among 19 CURGs. The PPI network was constructed using STRING v12 and visualized with Cytoscape. Based on the centrality score from Cytoscape, we identified key nodes in the PPI network, which led to the identification of *SLC31A1, ATP7A,* and *ATP7B* (Supplemental Fig. 1).

3.4. Validation of the expression of 19 CURGs in external datasets

To rigorously assess the accuracy of the diagnostic model comprising 19 CURGs, we performed external validation using two datasets (GSE16561 and GSE122709) sourced from the GEO database. Within the GSE16561 dataset, the *MTF1*, *HSPA1A*, *SCO2*, *ARF1*, *APP*, *MT1G*, and *NFE2L2* genes exhibited significantly elevated expression in the IS group (Fig. 3A). Similarly, in the GSE122709 dataset, the genes *DLD*, *ELP3*, *SCO2*, *ARF1*, *APP*, *SLC31A1*, *ANKRD9*, *HSF1*, and *NFE2L2* demonstrated increased expression levels in the IS group (Fig. 3B).

To assess the ability of the expression levels of 19 CURGs to distinguish between IS patients and non-IS patients, we conducted an ROC analysis. Notably, within the GSE16561 dataset, the AUC values for *MTF1*, *ELP3*, *HSPA1A*, *APP*, and *NFE2L2* exceeded 0.7, indicating robust discriminatory ability (Fig. 3C). Similarly, in the GSE122709 dataset, the AUC values for *DLD*, *CISD1*, *MTF1*, *ELP3*, *SCO2*, *ARF1*, *APP*, *SLC31A1*, *POLD1*, *ANKRD9*, *HSF1*, and *NFE2L2* > 0.7 (Fig. 3D), indicating the efficacy of these genes in distinguishing between IS and non-IS. These findings underscore the potential clinical utility of the 19 CURGs diagnostic model in predicting the likelihood of IS.

3.5. Gene set enrichment analysis (GSEA) and KEGG enrichment analysis of 19 CURGs

The GSEA results revealed significant enrichment patterns among various genes associated with different biological processes in IS. Notably, *DLD* was enriched in the NF−kappa B signaling pathway (Fig. 4A). *CISD1* was enriched in antigen processing and presentation, as well as Th1 and Th2 cell differentiation (Fig. 4B). *MTF1* was enriched in vascular smooth muscle contraction (Fig. 4C). *ELP3* was enriched in nitrogen metabolism (Fig. 4D). *HSPA1A* was enriched in neutrophil extracellular trap formation (Fig. 4E). *ATP7A* was enriched in oxidative phosphorylation (Fig. 4F), *PRNP* was enriched in protein export (Fig. 5A), *SCO2* and *ARF1* were both enriched in nitrogen metabolism (Fig. 5B–C), *COX19* was enriched in nitrogen metabolism and protein export (Fig. 5D), *APP* was enriched in axon guidance (Fig. 5E), *BECN1* was enriched in fatty acid biosynthesis (Fig. 5F), *SLC31A1* was enriched in phenylalanine metabolism (Fig. 6A), *POLD1* was enriched in the TNF signaling pathway (Fig. 6B), *ATP7B* was enriched in apoptosis and the Wnt signaling pathway (Fig. 6C), *MT1G* was enriched in protein export (Fig. 6D), *ANKRD9* was enriched in antigen processing and presentation (Fig. 6E), *HSF1* was enriched in protein export (Fig. 6F), and *NFE2L2* was enriched in protein transport and TNF signaling pathway (Fig. 7A). The results of GSEA offer fresh perspectives on how these genes contribute to IS pathophysiology and reveal their potential as treatment targets.

We utilized KEGG analysis to explore the biological functions of the 19 CURGs in IS. Our analysis revealed that these 19 CURGs have a significant impact on several crucial physiological and pathological processes involved in the occurrence and progression of IS. Specifically, our results highlighted the key roles played by these genes in the regulation of intracellular copper ion homeostasis, response to copper ion, response to metal ions, and copper ion transport (Fig. 7B).

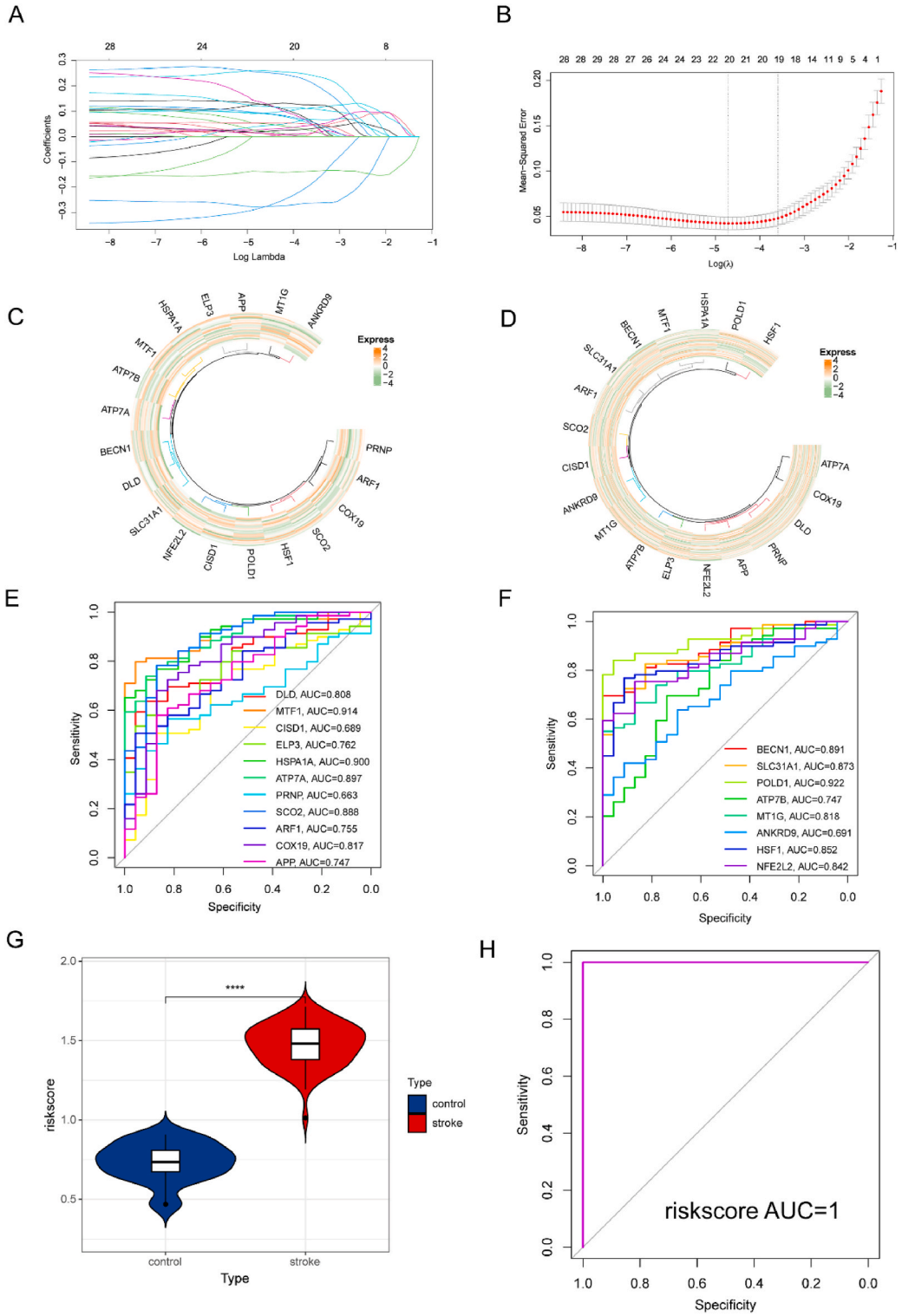

Fig. 2. Differential expression of 19 CURGs in the non-IS and IS groups; identification of the cuproptosis signature using the LASSO model. (A) LASSO coefficient profiles of variables. The vertical axis represents the estimated coefficients, while the horizontal axis is divided into two parts: the bottom axis represents the values of the regularization parameter log(λ), and the top axis represents the number of non-zero coefficients in the model given a specific log(λ) value. As the regularization parameter log λ increases, the regression coefficients (values on the vertical axis) gradually stabilize and eventually tend towards zero. (B) The cross-validation results. (C) The heatmap shows the expression levels of the 19 CURGs in the non-IS group, where yellow indicates high gene expression levels and green indicates low gene expression levels. (D) The heatmap illustrates the

expression levels of the 19 CURGs in the IS group, with yellow representing high gene expression levels and green representing low gene expression levels. (E–F) ROC curves were plotted for the 19 CURGs, evaluating their diagnostic accuracy. (G) Violin plot showing the cuproptosis-related risk score in the non-IS and IS groups. (H) The ROC curve illustrates the application of cuproptosis-related risk score in stratifying IS samples into high and low-risk groups. (For interpretation of the references to color in this figure legend, the reader is referred to the Web version of this article.)

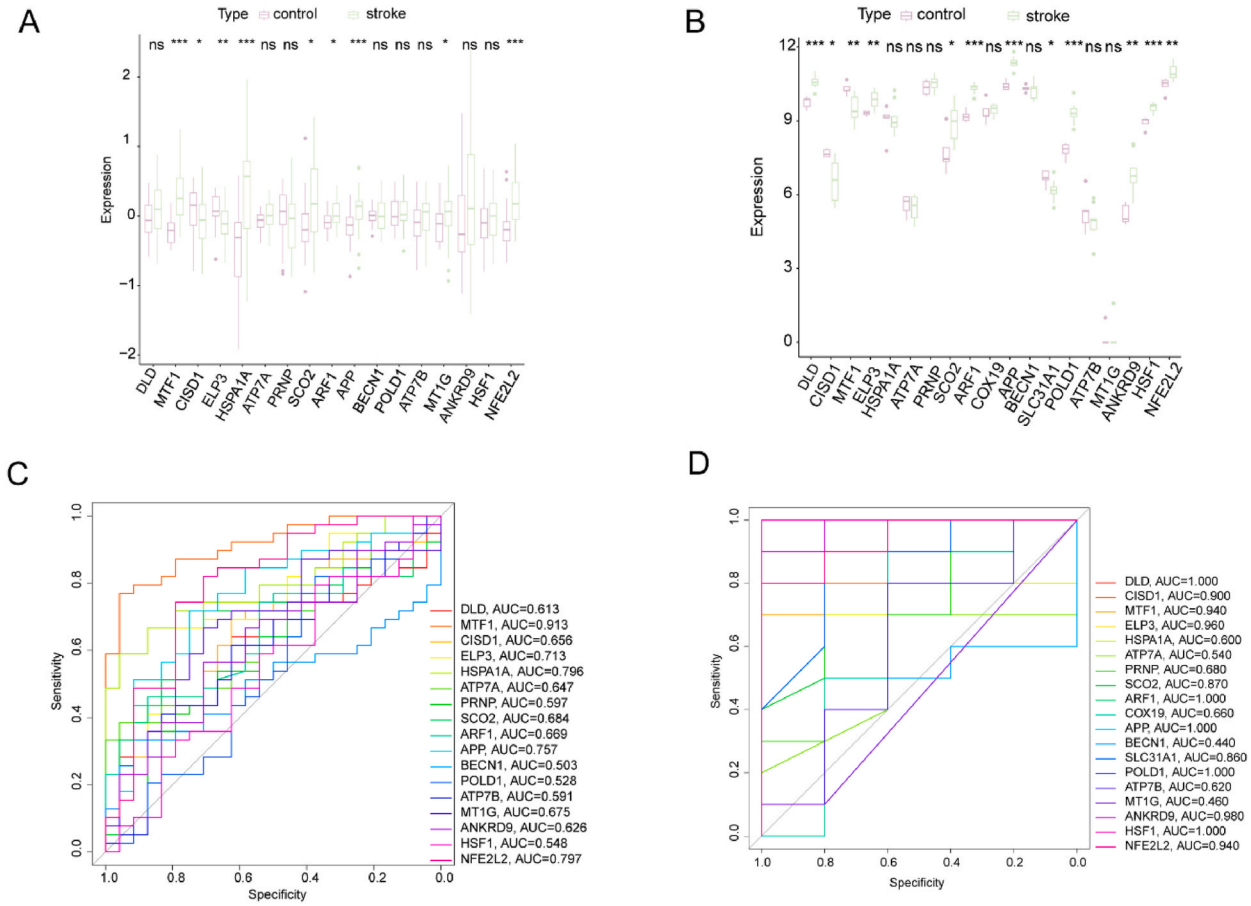

Fig. 3. Differential expression and diagnostic value of 19 CURGs in IS and non-IS patients. Boxplots and ROC analysis results for two independent datasets are shown: (A) GSE16561 and (B) GSE122709. The boxplots illustrate the distribution of expression levels of each CURG between the IS and non-IS groups. Statistical significance was determined by a Wilcoxon test (*, $P < 0.05$; **, $P < 0.01$; ***, $P < 0.001$; ****, $P < 0.0001$; ns, not significant). The ROC curves in (C) and (D) were generated to evaluate the diagnostic value of each CURG in discriminating between IS patients and non-IS patients in GSE16561 and GSE122709, respectively.

3.6. Single-cell analysis

In this study, we employed a single-cell analysis approach to investigate the expression patterns of 19 CURGs in mouse brain tissues. Specifically, one sample from an IS and one sample from a non-IS were selected for analysis. Through the integration and annotation of these samples using the SingleR software package and PanglaoDB database, we successfully identified and characterized 12 major cell types within the brain tissues (Fig. 8A).

To assess the differential expression of the 19 CURGs between the IS and non-IS groups, a bubble plot was generated, providing a visual representation of their expression patterns. Compared with those in the non-IS, the expression levels of *Dld*, *Cisd1*, *Prnp*, *Arf1*, and *Mt1* were significantly greater in the NK cells of the IS group. Granulocytes in the IS group presented higher expression levels of *Prnp* and *Mt1*. In the IS group, *Prnp*, *Arf1*, *App*, *Slc31a1*, and *Mt1* were expressed at higher levels in macrophages. Monocytes in the IS group displayed increased expression levels of *Dld*, *Cisd1*, *Prnp*, *Arf1*, *App*, *Becn1*, *Slc31a1*, and *Mt1*. Furthermore, microglia in the IS group presented increased expression levels of *Dld*, *Cisd1*, *Hspala*, *Atp7a*, *Prnp*, *Sco2*, *Arf1*, *Cox19*, *App*, *Becn1*, *Slc31a1*, and *Mt1* (Fig. 8B).

In addition, we employed the AUCell score to further explore the expression of gene sets associated with natural killer cell-mediated cytotoxicity, steroid hormone biosynthesis, and oxidative phosphorylation in the IS. These findings provide novel insights into the potential involvement of these gene sets in the pathophysiology of IS (Fig. 8C–E).

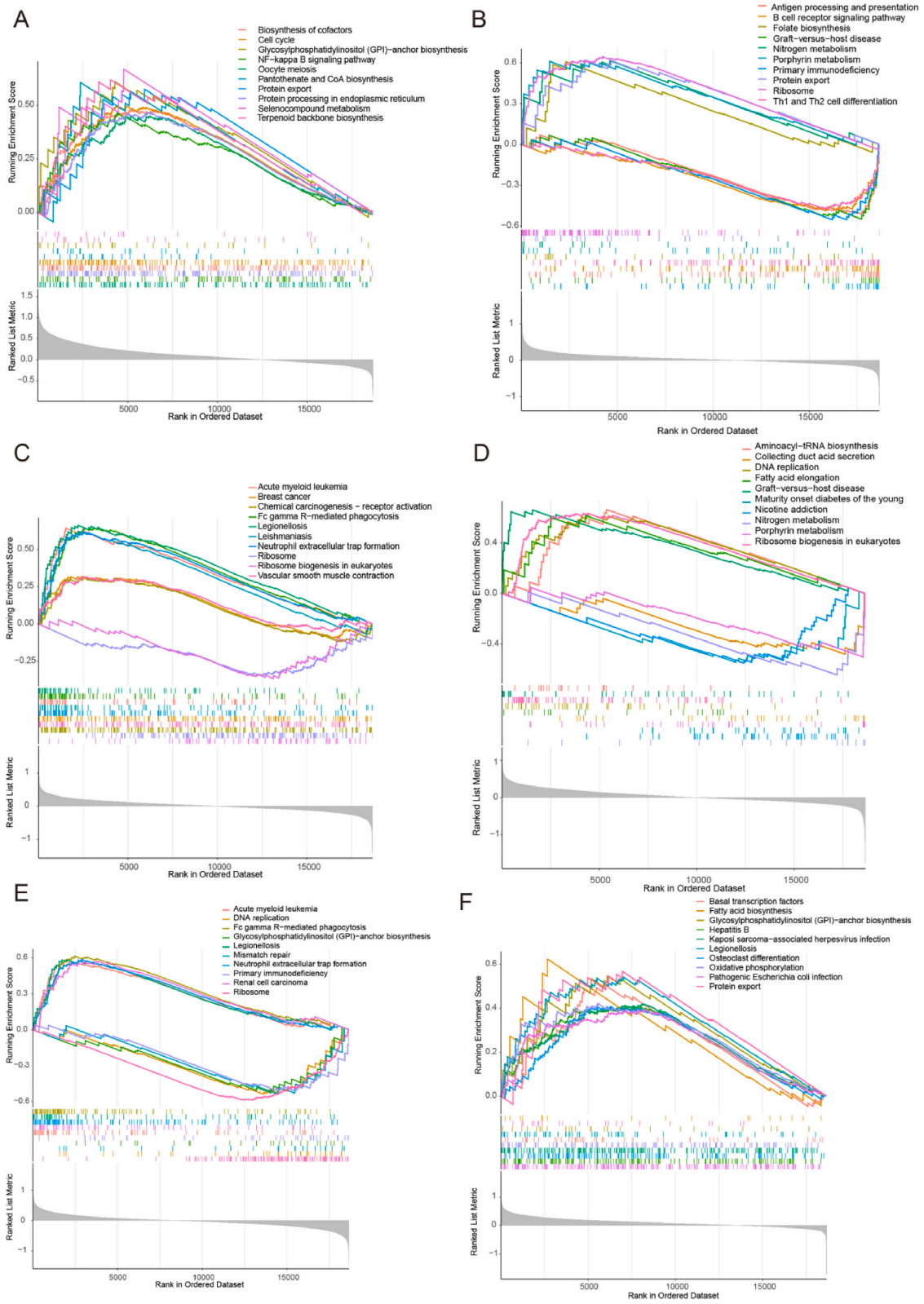

Fig. 4. Gsea of CURGs. (A) *DLD*, (B) *CISD1*, (C) *MTF1*, (D) *ELP3*, (E) *HSPA1A*, (F) *ATP7A*.

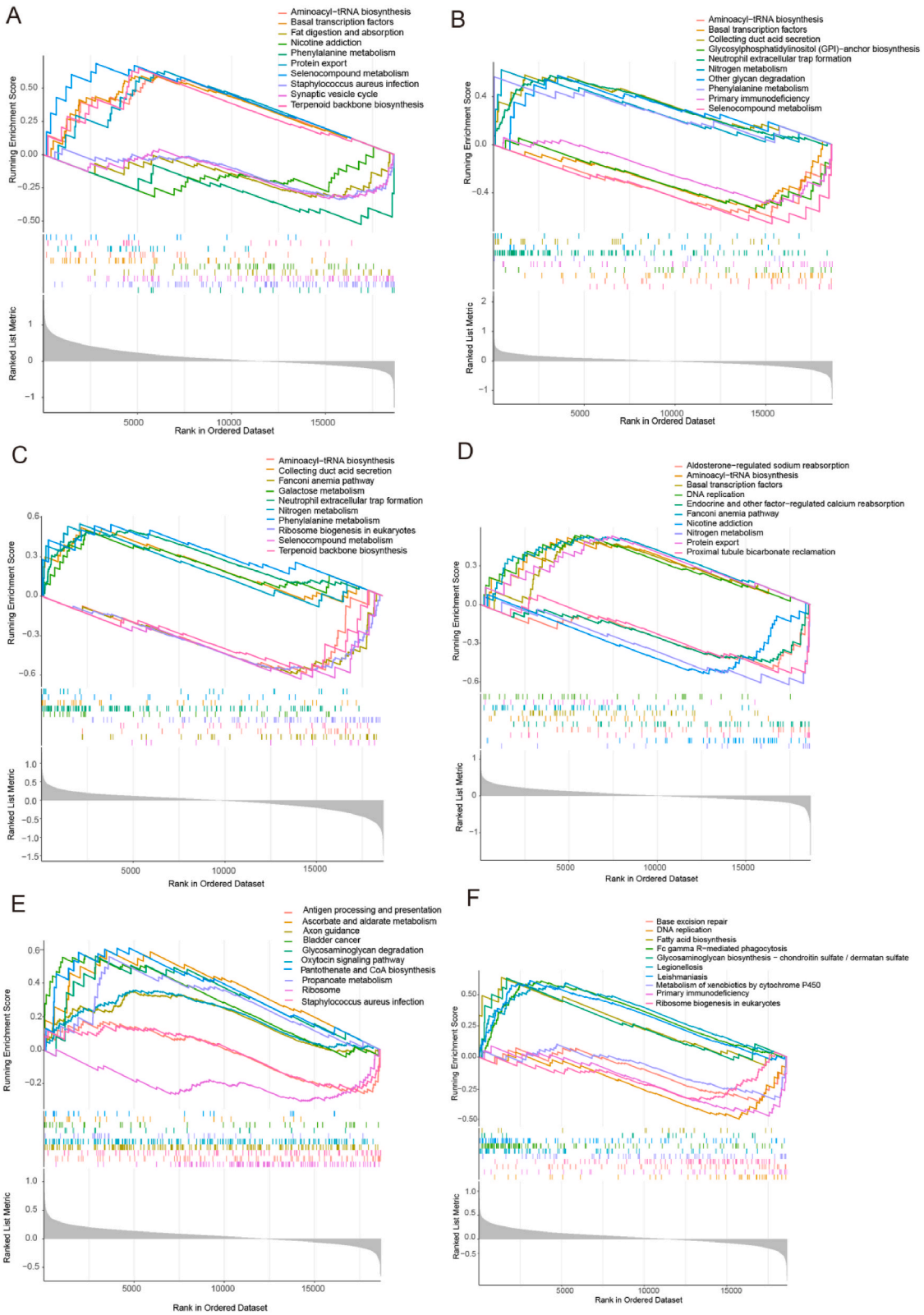

Fig. 5. Gsea of CURGs. (A) *PRNP*, (B) *SCO2*, (C) *ARF1*, (D) *COX19*, (E) *APP*, and (F) *BECN1*.

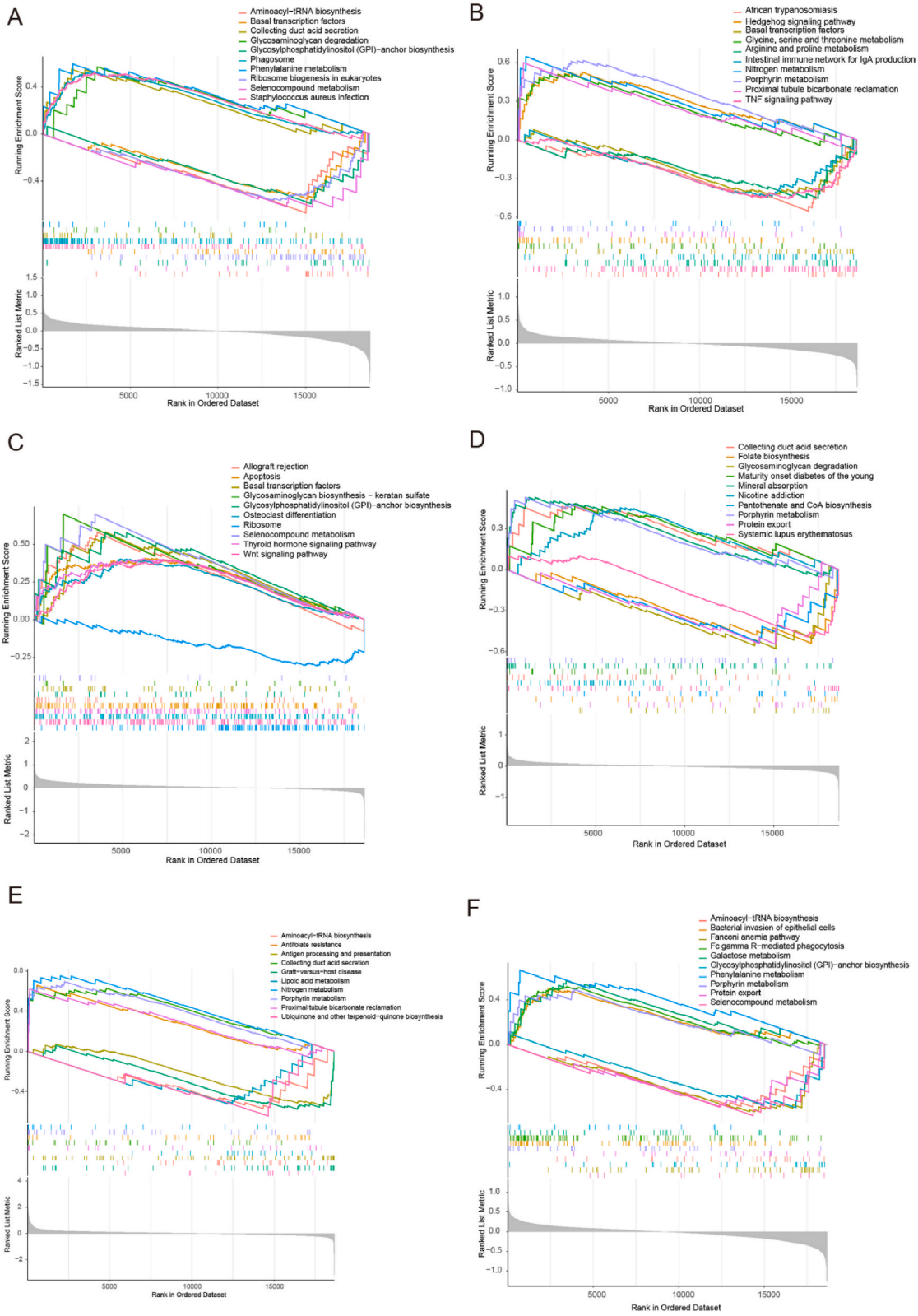

Fig. 6. Gsea of CURGs. (A) *SLC31A1*, (B) *POLD1*, (C) *ATP7B*, (D) *MT1G*, (E) *ANKRD9*, and (F) *HSF1*.

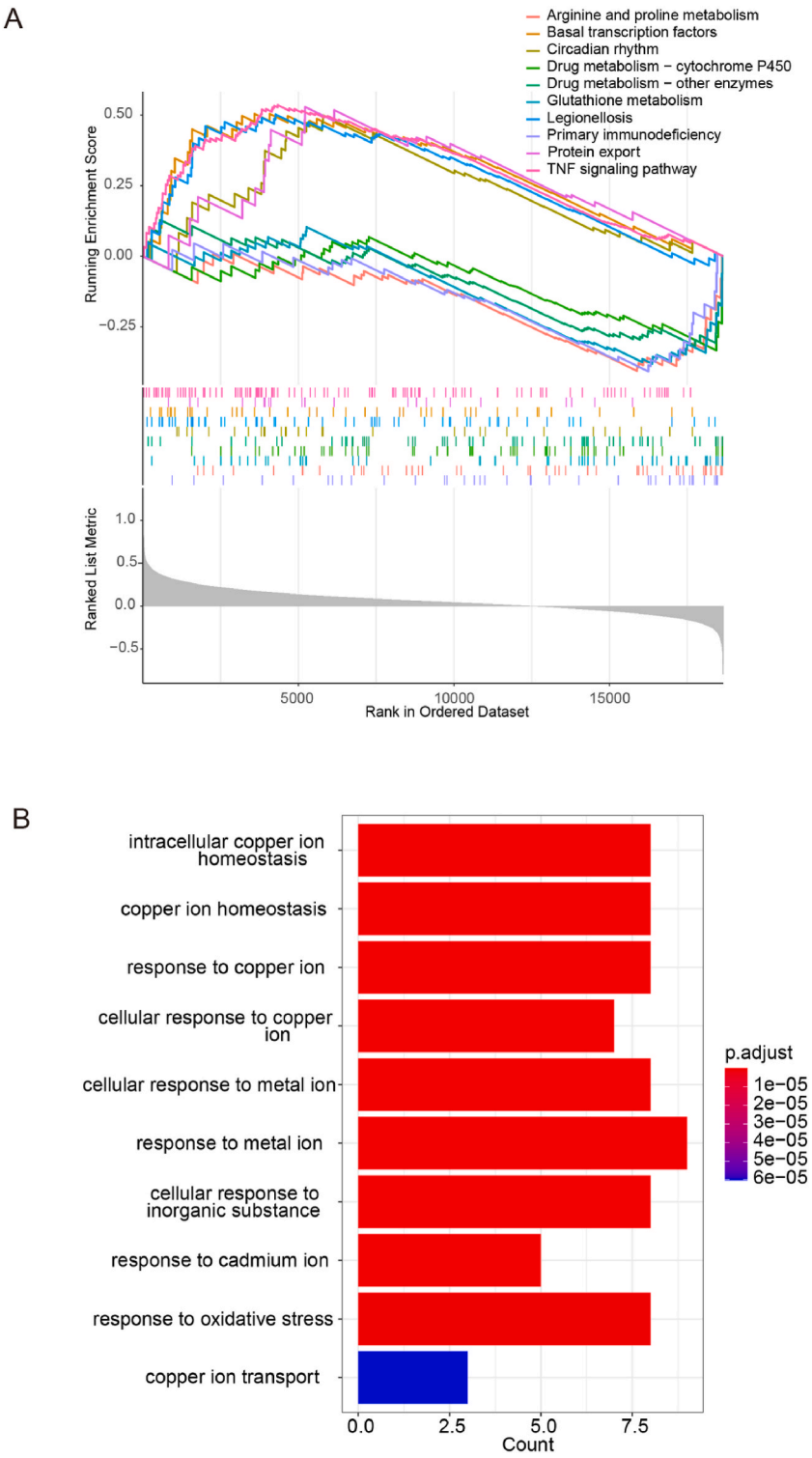

Fig. 7. GSEA and KEGG analysis of the CURGs. (A) GSEA of *NFE2L2*, (B) KEGG analysis of 19 CURGs.

3.7. Immune infiltration analysis

We also conducted an immune infiltration analysis to evaluate the differences in the proportions of 22 immune cell types between the IS and non-IS groups. Notably, there were significant differences observed between the two groups, particularly in plasma cells,

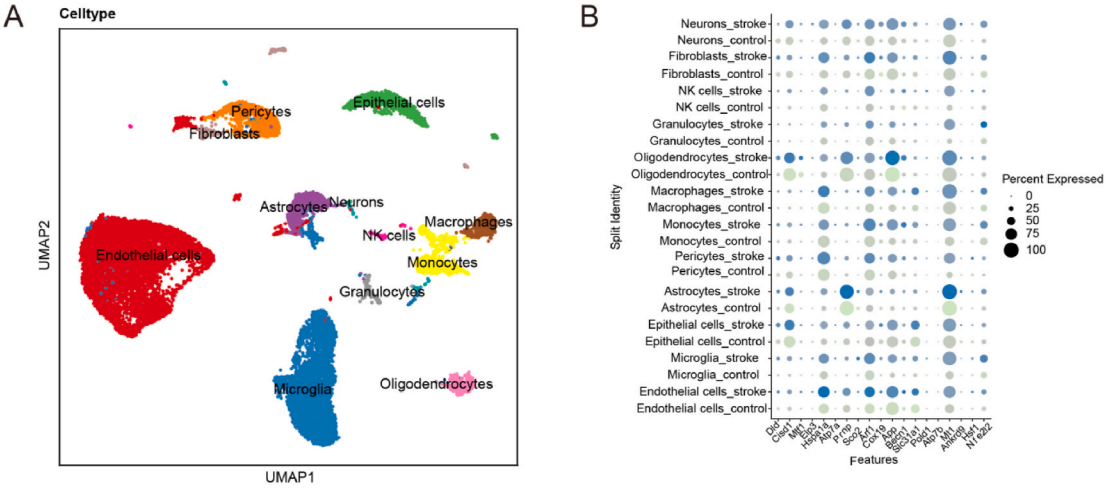

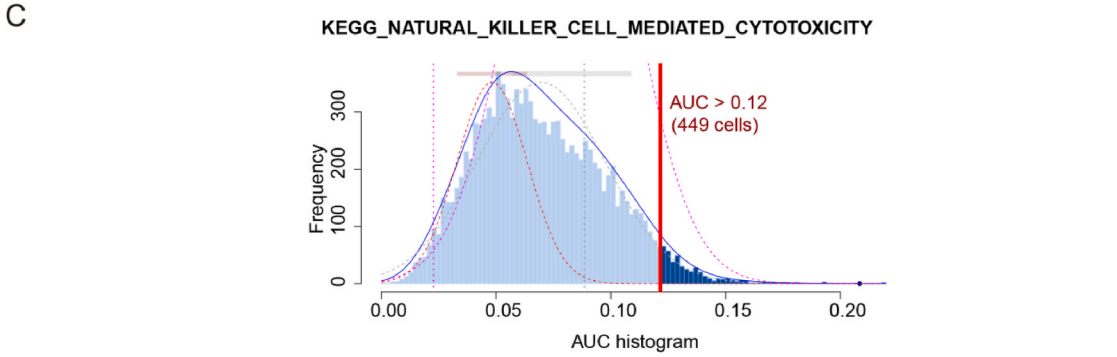

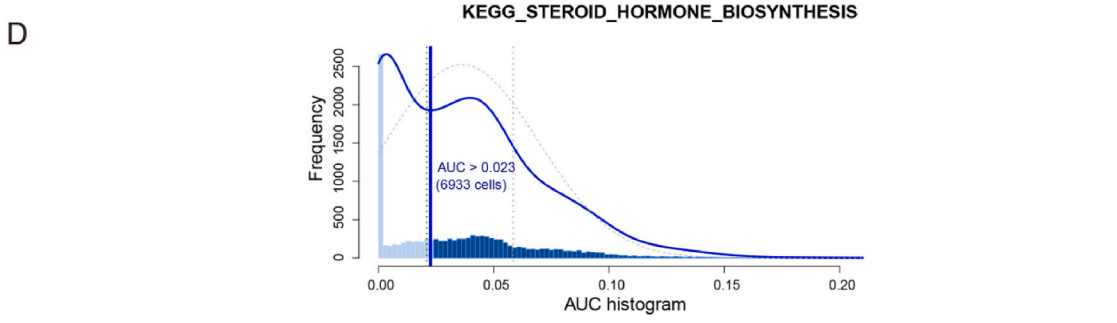

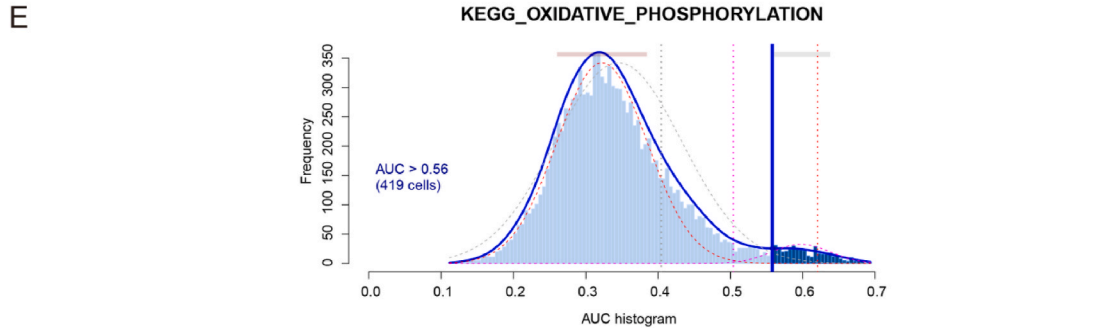

(caption on next page)

Fig. 8. Integrated analysis of 10x scRNA-seq data from IS and non-IS samples (A) Cell type identification using UMAP revealed distinct colors representing different cell types. (B) Bubble plot showing the differences in the expression of 19 CURGs across various cell types in IS and non-IS samples. (C) Natural killer cell-mediated cytotoxicity pathway activity. (D) Steroid hormone biosynthesis pathway activity. (E) Oxidative phosphorylation pathway activity. scRNA-seq: single-cell RNA sequencing; UMAP: unified flowform approximation and projection. (For interpretation of the references to color in this figure legend, the reader is referred to the Web version of this article.)

naive CD4^{+} T cells, activated dendritic cells, and neutrophils (Fig. 9A). We analyzed the correlations between four immune cell types and 19 CURGs. Our findings indicated that most of the 19 CURGs were significantly correlated with the four immune cell types (Fig. 9B).

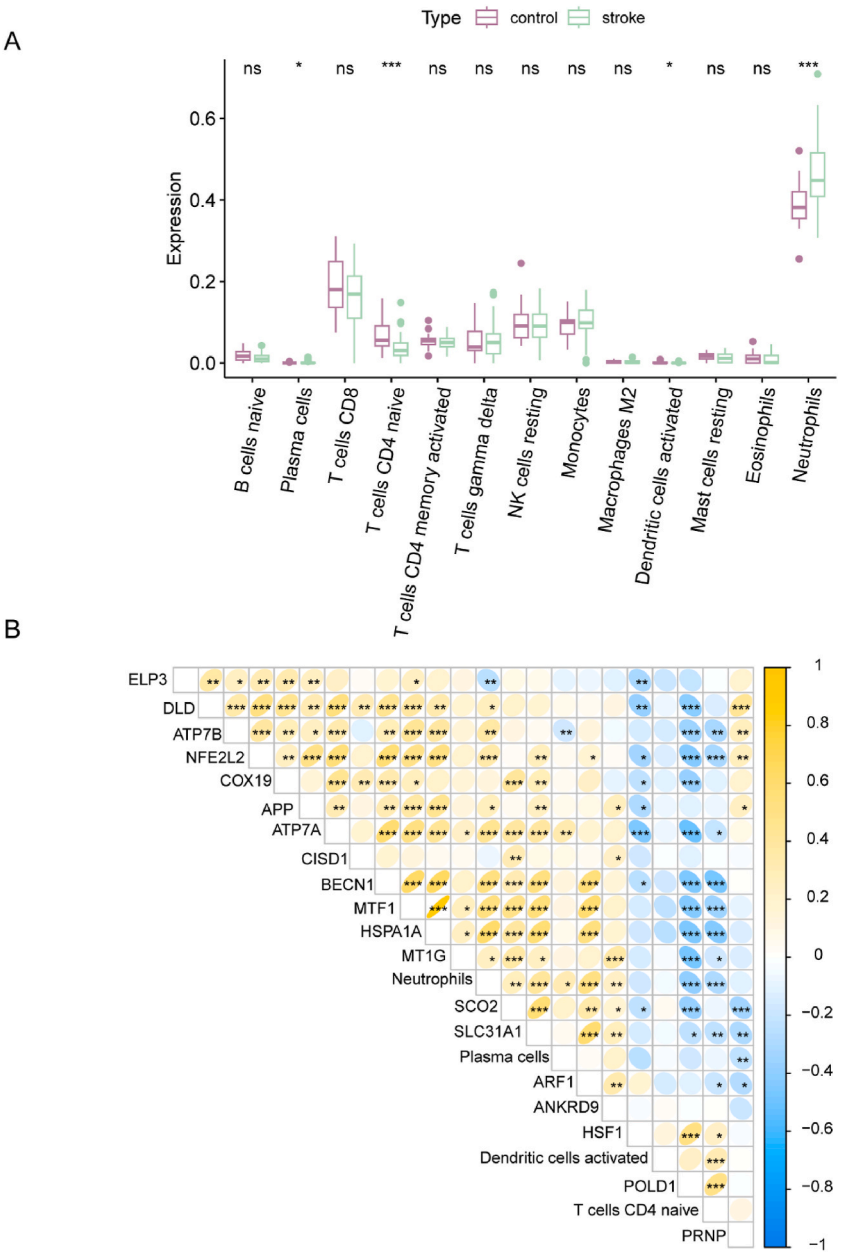

Fig. 9. Assessment of immune cell counts in the 19 CURGs and correlation analysis of 19 CURGs and immune cells. (A) Boxplot illustrating the expression levels of immune cells in the non-IS and IS groups. (B) The heatmap shows the relationships between the 19 CURGs and four distinct immune cell types, with negative correlations marked in blue and positive correlations in yellow (*, $P < 0.05$; **, $P < 0.01$; ***, $P < 0.001$; ****, $P < 0.0001$; ns, not significant). (For interpretation of the references to color in this figure legend, the reader is referred to the Web version of this article.)

3.8. WGCNA network construction of IS and non-IS patients

In this study, a WGCNA network was used to identify module genes associated with IS. Further investigation was conducted using a scale-free R^2 of 0.9 and a β value of 14 (Fig. 10A). The data were divided into several modules, with the red module being particularly relevant to the IS (Fig. 10B). The red module genes were selected for KEGG pathway enrichment, revealing their prevalence in neurological disorders, including Parkinson's, Huntington's, and Alzheimer's disease (Fig. 10C).

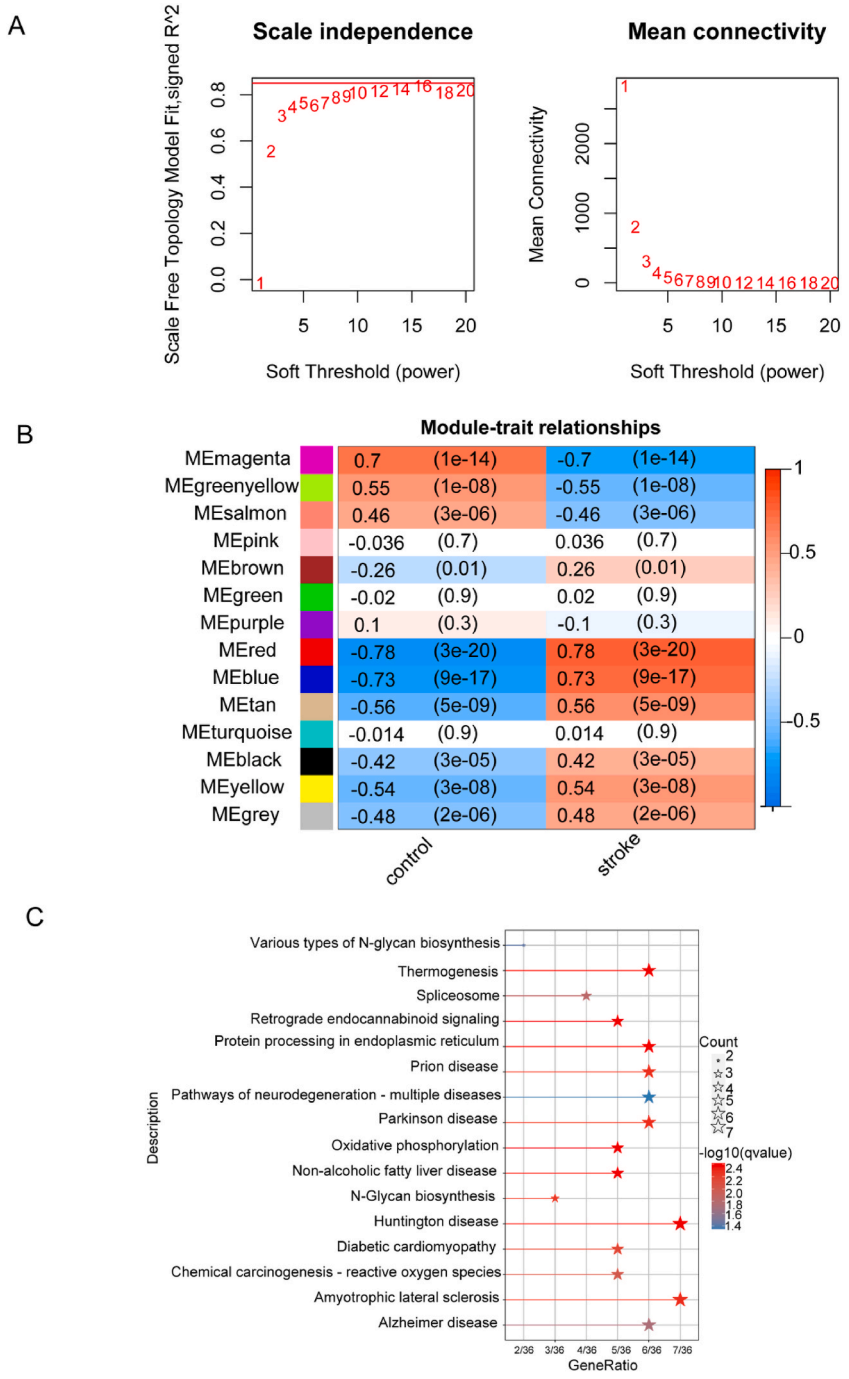

Fig. 10. WGCNA in IS for identification of characteristic genes and KEGG pathway analysis of the core module associated with IS. (A) Evaluation of the scale-free indices for different β values and mean connectivity across various β values. (B) Heatmap depicting the correlation between module eigengenes and clinical traits. (C) KEGG pathway analysis related to the genes within the MEred-grade block.

3.9. Time series analysis of IS

The IS expression matrix from GSE58294 was separated into three groups (3 h, 5 h, and 24 h) for time series analysis. The data were then organized into eight clusters (Fig. 11A, Supplementary Materials 2), with different gene sets showing changes over time. The changes in the expression of the 19 CURGs were also examined at these time points. *MTF1*, *CISD1*, *RRNP*, *SCO2*, *ARF1*, *APP*, *SLC31A1*, and *NFE2L2* were found in cluster 1; *ATP7B*, *MT1G*, *ANKRD9*, and *HSF1* were found in cluster 2; and *HSPA1A*, *ATP7A*, and *BECN1* were found in cluster 3. Finally, *DLD*, *ELP3*, *COX19*, and *POLD1* were included in cluster 4 (Fig. 11B).

3.10. Clusters of CURGs identified in IS

Using the consensus clustering method, 19 CURGs were categorized into two clusters with high expression in cluster 2 (Fig. 12A–B), excluding *CISD1*, *SCO2*, *ARF1*, *SLC31A1*, *POLD1*, and *ANKRD9* (Fig. 12C). The 69 IS samples were divided into low (n = 39) and high (n = 30) expression clusters, which represented different immune microenvironments. There were significant differences in the types of immune cells present, such as naive B cells, plasma cells, resting NK cells, resting mast cells, and eosinophils, between the two clusters (Fig. 12D).

3.11. GSVA and functional analysis

Differential pathways related to IS were identified through GSVA. Cluster 2 exhibited increased activity in the NFKB, TGF-β, and Notch signaling pathways (Fig. 13A), while Cluster 1 exhibited activity in the coagulation and Kras signaling pathways (Fig. 13B). We further conducted a differential expression analysis, identifying 123 DEGs (48 upregulated and 75 downregulated) in the two clusters, and performing GO and KEGG analyses. GO analysis revealed that the DEGs were predominantly enriched in myeloid cell differentiation, myeloid cell homeostasis, and oxygen transport, whereas no enrichment was observed in the KEGG analysis (Fig. 13C).

4. Discussion

Stroke is a debilitating disease with limited treatment options and is currently restricted by the need for intravenous thrombolysis or mechanical thrombectomy. However, strict eligibility criteria limit the applicability of these time-sensitive therapies to only a small number of patients, highlighting the pressing need for new treatments that can benefit a wider range of stroke patients [42]. Cuproptosis is a recently discovered cell death process in which copper binds to lipoxygenase in the tricarboxylic acid cycle. This mechanism has been shown to have an important impact on the progression and severity of stroke [18]. Previous research has suggested that serum copper concentration is a potential risk factor for IS [23]. Additionally, the study of immune infiltration in IS may provide a promising and novel approach for exploring treatment options given the immune system's role in repair following stroke [43]. Elevated levels of the small molecules of copper and total copper were observed in the serum of patients with IS [44].

The GEO database was used to obtain IS samples, which were subsequently divided into two clusters: cluster 1 and cluster 2.

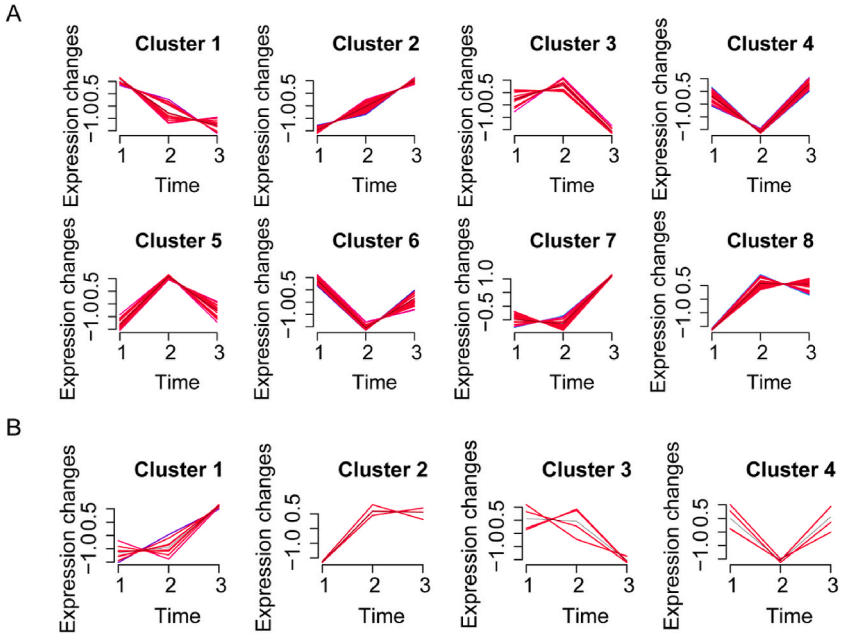

Fig. 11. Time series data for gene expression at three time points, including (A) GSE58294. (B) 19 CURGs.

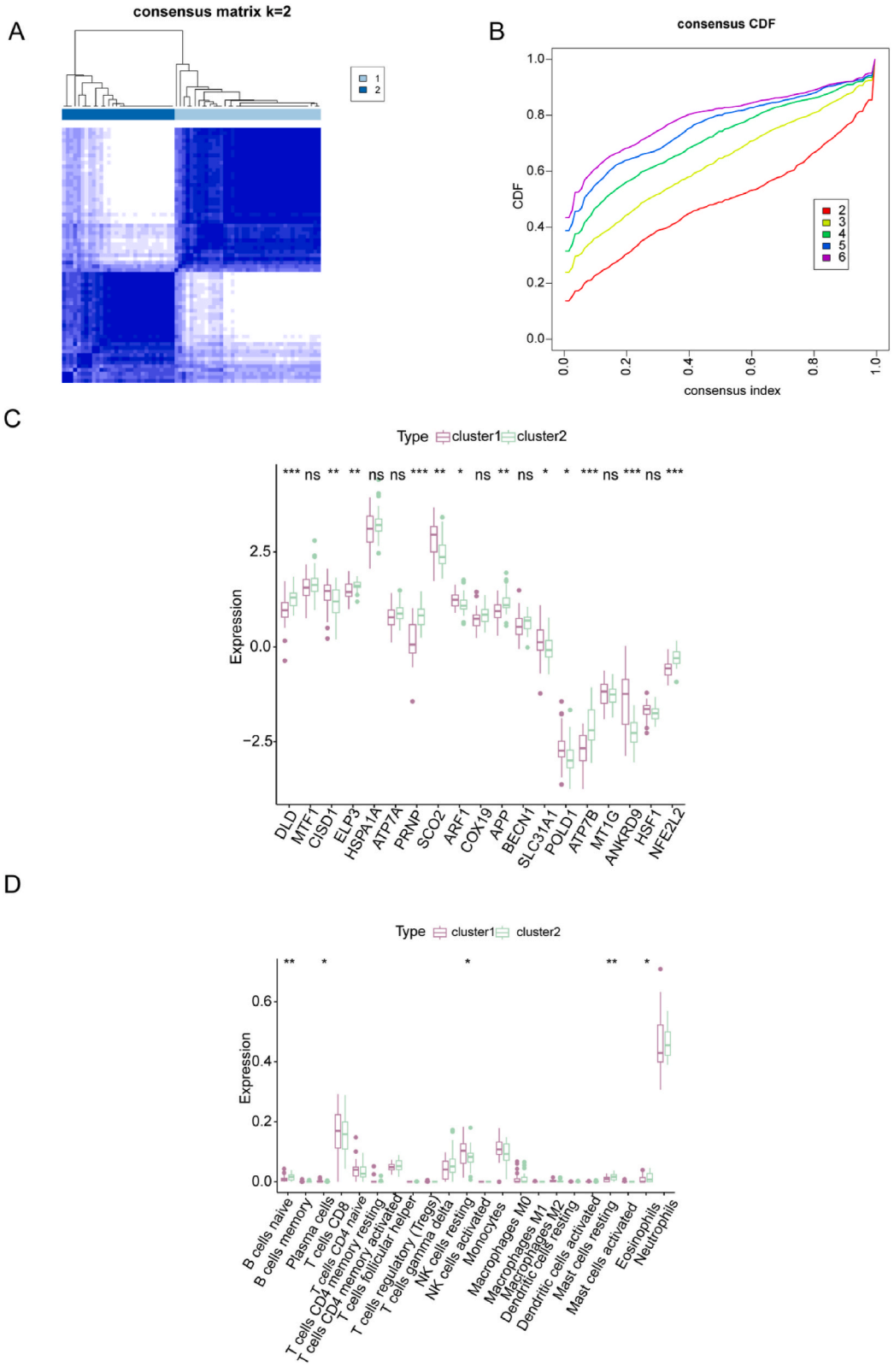

(caption on next page)

Fig. 12. Consensus clustering analysis revealed two distinct clusters within the IS sample. (A) The consensus matrix heatmap (k = 2) revealed the correlation region of these two clusters. (B) The region with a relative change in the expression below the cumulative distribution function curve also confirms this division. (C). The expression of 19 CURGs was distinctly different between the two clusters. (D). There was variation in the immune cell expression profiles between these two clusters (*, $P < 0.05$; **, $P < 0.01$; ***, $P < 0.001$; ****, $P < 0.0001$; ns, not significant).

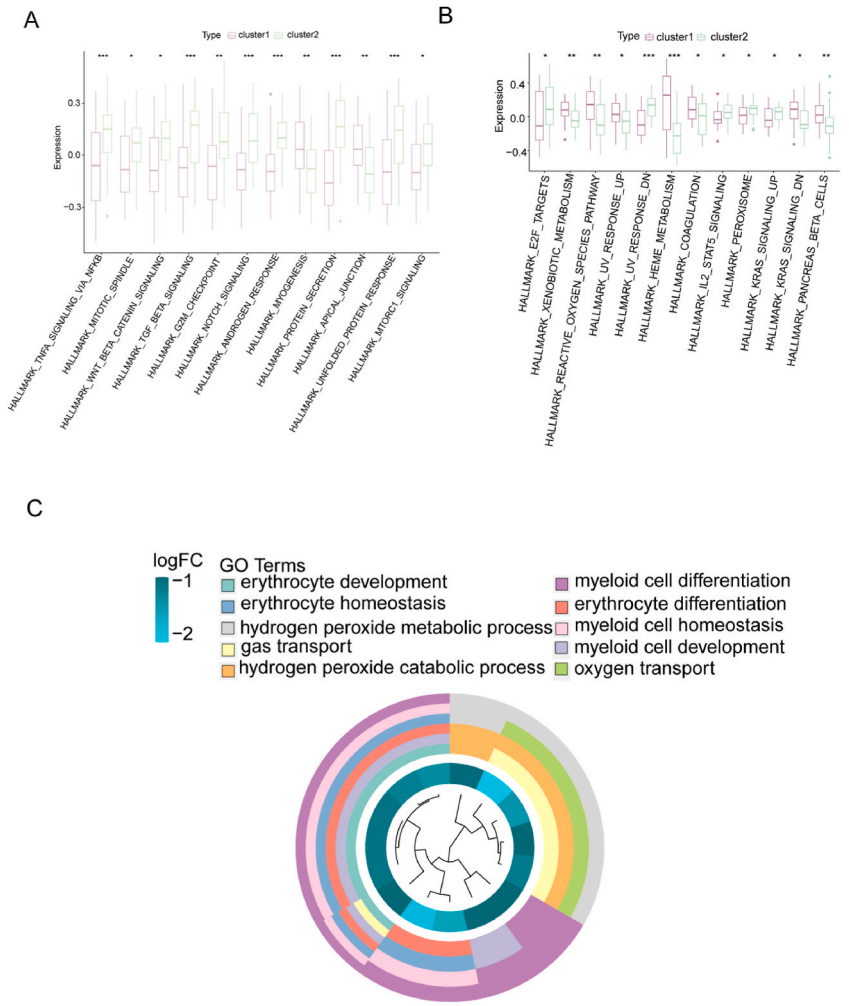

Fig. 13. GSVA and GO analysis of the two clusters. (A) Comparative results of GSVA depicting 12 key pathway activities between the two clusters (*, $P < 0.05$; **, $P < 0.01$; ***, $P < 0.001$; ****, $P < 0.001$; ns, not significant). (B) Comparative results of GSVA depicting another 12 key pathway activities between the two clusters (*, $P < 0.05$; **, $P < 0.01$; ***, $P < 0.001$; ****, $P < 0.001$; ns, not significant). (C) Functional enrichment results from GO analysis illustrate the DEGs in the two clusters.

Notably, the identified clusters exhibited differential immune infiltration and functions, as did the various CURG compositions. Through further GSVA, we observed differences between the two clusters. Specifically, cluster 1 exhibited activity in coagulation signaling pathways, while cluster 2 exhibited enhancement of the NF-κB, TGF-β, p53, and Notch signaling pathways. All these pathways are closely associated with stroke. A hypercoagulable state may lead to a potentially high risk of stroke [45]. The NF-κB signaling pathway controls immune system genes and is involved in poststroke repair processes [46]. The TGF-β signaling pathway promotes angiogenesis and inhibits apoptosis, while the Notch signaling pathway enhances neuronal stem cell survival following stroke [47,48].

The study highlighted the correlation between IS and heightened levels of neutrophils, which is supported by previous research. Specifically, neutrophils are recruited because of an inflammatory reaction following IS. Additionally, the ratio of neutrophils to lymphocytes can be utilized to predict both hemorrhagic transformation and clinical outcomes of stroke [49,50]. In the present study, unsupervised clustering analysis was employed to classify patients afflicted with IS into two discernible clusters. This classification was based on the expression of 19 CURGs. Notably, a differential distribution of immune cells was observed between the clusters, with cluster 1 displaying higher levels of resting NK cells, while cluster 2 exhibiting elevated amounts of naive B cells, plasma cells, and

resting mast cells. These findings underscore the potential significance of the immune microenvironment in the pathogenesis of IS, highlighting the need for further exploration of the underlying mechanisms involved.

Machine learning models are increasingly being used to predict the prevalence of IS. We analyzed 19 CURG features via ROC curves, which demonstrated high diagnostic ability (AUC = 1) for predicting IS. The increased relative risk of cuproptosis in the IS group compared to the non-IS group suggested that CURGs have a significant impact on the development and advancement of IS. Research indicates that metal responsive transcription factor 1 (MTF-1) triggers the *NCX1* brain promoter, which assists in preventing neurodegeneration after stroke [51]. During ischemia, cerebral blood flow interruption leads to mitochondrial oxidative phosphorylation dysfunction and bioenergetic stress. *CISD1* is involved primarily in regulating mitochondrial iron uptake and respiratory capacity [52]. *DLD* plays a crucial role as an enzyme in various complexes such as dehydrogenase and glycine decarboxylase, which are responsible for regulating cellular and mitochondrial homeostasis [53].

Reducing the phosphorylation of *BECN1* after cerebral infarction can alleviate vascular lysosomal degradation dysfunction in IS and promote thalamic angiogenesis and secondary nerve repair [54]. *SLC31A1* and *SCO2* play crucial roles in maintaining cellular copper homeostasis [55,56]. *NFE2L2* is a potential therapeutic target that can alleviate harmful oxidative events in the ischemic cascade by regulating the expression of several antioxidant and defense proteins [57]. Copper imbalance is a significant contributor to various neurodegenerative diseases. Studies suggest that *MT1G*, *ATP7A*, *APP*, and *ATP7B* may contribute to neurodegenerative disease [58–61]. *ELP3* is associated with neurodevelopmental disorders [62]. *HSPA1A* plays a vital role in regulating neuroinflammatory responses after IS [63]. Our study revealed that *SLC31A1, ATP7A,* and *ATP7B* are hub genes involved in IS. These findings align with those of a previous study that demonstrated that *SLC31A1* mediates copper uptake while *ATP7A/B* exports copper, indicating that an imbalance in copper homeostasis can lead to cell death and potentially cause stroke [64]. Our findings suggest that CURGs could function as predictive biomarkers for IS. In the future, immunotherapy could be combined with CURGs to develop a novel therapy for improving clinical outcomes in IS patients. Through GSEA and AUCell analyses, we found that these cuproptosis-related genes were enriched in the NF-κB signaling pathway, oxidative phosphorylation pathway, and TNF signaling pathway, suggesting that they are closely associated with microglial function. Additionally, research has demonstrated that the NF-kB signaling pathway can attenuate the inflammatory response of microglia [65], and modulation of this pathway can improve post-IS motor function by regulating microglial polarization [66]. Furthermore, microglia are involved in regulating oxidative phosphorylation processes [67] and can participate in IS pathogenesis by modulating TNF expression [68]. These findings highlight the strong correlation between the expression of CURGs and microglial function, as well as the role of CURG expression in the pathophysiology of IS.

In our study, we employed GSEA to detect enriched gene sets associated with specific biological processes, revealing coordinated changes in gene expression. Additionally, we utilized the KEGG database for in-depth pathway analysis, elucidating the molecular functions and interactions among genes within biological pathways. The use of the AUCell package allowed us to identify cells with active gene sets within single-cell datasets. Through single-cell analysis, we dissected the heterogeneity of cell populations, uncovering new cell subtypes and states. We also applied consensus clustering, a statistical analysis method based on multiple clustering results, to enhance the stability and reliability of the clustering outcomes. The combined application of these methods represents the novelty of our research, providing a comprehensive and multidimensional analytical perspective on the role of CURGs in IS.

To strengthen the validity of our analysis, additional investigations beyond bioinformatics are essential. Conducting *in vivo* and *in vitro* experiments is critical for validating the expression levels of these genes and confirming our findings. Furthermore, developing a more comprehensive prediction model that integrates detailed clinical features can enhance its precision. A larger sample size of IS samples is needed to accurately determine the clusters associated with cuproptosis. It is also imperative to explore the relationship between CURGs and the immune response to gain insights into their role in the progression of IS. While our study identified the expression of CURGs in microglia and suggested their potential association with the pathophysiology of IS, we have yet to fully validate the precise mechanisms of action of these genes in microglial function and their correlation with pathological markers of IS. Future studies may involve large-scale prospective cohort designs coupled with biomarker measurements, providing deeper insights into the metabolic dynamics of copper in the body and aiming to comprehensively understand the relationship between copper intake and susceptibility to stroke.

5. Conclusion

Our study highlights the role of CURGs in IS by connecting them to immune cell infiltration and identifying distinct subtypes with a 19 CURGs signature. This research is crucial for advancing future scientific investigations and the development of targeted treatments for IS.

Funding

This study was supported by grants from the National Natural Science Foundation of China (82271371 and 82260367), the High-Level Medical Expert Training Program of Guangxi "139" Plan Funding, the Guangxi Medical and Health Appropriate Technology Development and Application Project (S2021107), the Clinical Research "Climbing" Program of the First Affiliated Hospital of Guangxi Medical University (YYZS2021002), the Advanced Innovation Teams and Xinghu Scholars Program of Guangxi Medical University, and the Innovation Project of Guangxi Graduate Education (YCSW2023242).

Data availability statement

Data will be made available on request.

CRediT authorship contribution statement

Rongxing Qin: Writing – review & editing, Writing – original draft, Validation, Software, Methodology, Investigation, Formal analysis, Data curation, Conceptualization. **Xiaojun Liang:** Writing – review & editing, Writing – original draft, Validation. **Yue Yang:** Writing – review & editing, Writing – original draft. **Jiafeng Chen:** Writing – review & editing, Writing – original draft. **Lijuan Huang:** Writing – review & editing, Writing – original draft. **Wei Xu:** Writing – review & editing, Writing – original draft. **Qingchun Qin:** Writing – review & editing, Writing – original draft. **Xinyu Lai:** Writing – review & editing, Writing – original draft. **Xiaoying Huang:** Writing – review & editing, Writing – original draft. **Minshan Xie:** Writing – review & editing, Writing – original draft. **Li Chen:** Writing – review & editing, Writing – original draft, Supervision, Methodology, Funding acquisition, Formal analysis, Data curation, Conceptualization.

Declaration of competing interest

The authors declare that they have no known competing financial interests or personal relationships that could have appeared to influence the work reported in this paper.

Appendix A. Supplementary data

Supplementary data to this article can be found online at https://doi.org/10.1016/j.heliyon.2024.e36559.

References

[1] M. Vijayan, P.H. Reddy, Stroke, vascular dementia, and alzheimer's disease: molecular links, J. Alzheim. Dis. : JAD. 54 (2016) 427–443.
[2] V.L. Feigin, G. Nguyen, K. Cercy, C.O. Johnson, T. Alam, P.G. Parmar, A.A. Abajobir, K.H. Abate, F. Abd-Allah, A.N. Abejie, et al., Global, regional, and country-specific lifetime risks of stroke, 1990 and 2016, N. Engl. J. Med. 379 (2018) 2429–2437.
[3] K. Bhatia, L.M. Ladd, K.H. Carr, M. Di Napoli, J.L. Saver, L.D. McCullough, M. Hosseini Farahabadi, D.L. Alsbrook, A. Hinduja, J.G. Ortiz Garcia, et al., Contemporary antiplatelet and anticoagulant therapies for secondary stroke prevention: a narrative review of current literature and guidelines, Curr. Neurol. Neurosci. Rep. 23 (2023) 235–262.
[4] V.L. Feigin, M. Brainin, B. Norrving, S. Martins, R.L. Sacco, W. Hacke, M. Fisher, J. Pandian, P. Lindsay, World stroke organization (WSO): global stroke fact sheet 2022, Int. J. Stroke 17 (2022) 18–29.
[5] Y. Zhao, X. Hua, X. Ren, M. Ouyang, C. Chen, Y. Li, X. Yin, P. Song, X. Chen, S. Wu, et al., Increasing burden of stroke in China: a systematic review and meta-analysis of prevalence, incidence, mortality, and case fatality, Int. J. Stroke 18 (2023) 259–267.
[6] L. Wang, X. Zhang, X. Xiong, H. Zhu, R. Chen, S. Zhang, G. Chen, Z. Jian, Nrf2 regulates oxidative stress and its role in cerebral ischemic stroke, Antioxidants 11 (2022).
[7] J. Emberson, K.R. Lees, P. Lyden, L. Blackwell, G. Albers, E. Bluhmki, T. Brott, G. Cohen, S. Davis, G. Donnan, et al., Effect of treatment delay, age, and stroke severity on the effects of intravenous thrombolysis with alteplase for acute ischaemic stroke: a meta-analysis of individual patient data from randomised trials, Lancet (London, England) 384 (2014) 1929–1935.
[8] J.L. Saver, M. Goyal, A. van der Lugt, B.K. Menon, C.B. Majoie, D.W. Dippel, B.C. Campbell, R.G. Nogueira, A.M. Demchuk, A. Tomasello, et al., Time to treatment with endovascular thrombectomy and outcomes from ischemic stroke: a meta-analysis, JAMA 316 (2016) 1279–1288.
[9] R. Jahan, J.L. Saver, L.H. Schwamm, G.C. Fonarow, L. Liang, R.A. Matsouaka, Y. Xian, D.N. Holmes, E.D. Peterson, D. Yavagal, E.E. Smith, Association between time to treatment with endovascular reperfusion therapy and outcomes in patients with acute ischemic stroke treated in clinical practice, JAMA 322 (2019) 252–263.
[10] L. Ramiro, A. Simats, T. García-Berrocoso, J. Montaner, Inflammatory molecules might become both biomarkers and therapeutic targets for stroke management, Ther Adv Neurol Disord 11 (2018) 1756286418789340.
[11] R.C. Coll, K. Schroder, P. Pelegrín, NLRP3 and pyroptosis blockers for treating inflammatory diseases, Trends Pharmacol. Sci. 43 (2022) 653–668.
[12] B.R. Stockwell, J.P. Friedmann Angeli, H. Bayir, A.I. Bush, M. Conrad, S.J. Dixon, S. Fulda, S. Gascón, S.K. Hatzios, V.E. Kagan, et al., Ferroptosis: a regulated cell death nexus linking metabolism, redox biology, and disease, Cell 171 (2017) 273–285.
[13] X. Fan, H. Chen, F. Jiang, C. Xu, Y. Wang, H. Wang, M. Li, W. Wei, J. Song, D. Zhong, G. Li, Comprehensive analysis of cuproptosis-related genes in immune infiltration in ischemic stroke, Front. Neurol. 13 (2022) 1077178.
[14] D. Guan, L. Zhao, X. Shi, X. Ma, Z. Chen, Copper in cancer: from pathogenesis to therapy, Biomed. Pharmacother. 163 (2023) 114791.
[15] P. Tsvetkov, S. Coy, B. Petrova, M. Dreishpoon, A. Verma, M. Abdusamad, J. Rossen, L. Joesch-Cohen, R. Humeidi, R.D. Spangler, et al., Copper induces cell death by targeting lipoylated TCA cycle proteins, Science (New York, N.Y.) 375 (2022) 1254–1261.
[16] L. Chen, J. Min, F. Wang, Copper homeostasis and cuproptosis in health and disease, Signal Transduct. Targeted Ther. 7 (2022) 378.
[17] J. Zhang, J. Cao, H. Zhang, C. Jiang, T. Lin, Z. Zhou, Y. Song, Y. Li, C. Liu, L. Liu, et al., Plasma copper and the risk of first stroke in hypertensive patients: a nested case-control study, Am. J. Clin. Nutr. 110 (2019) 212–220.
[18] X. Chen, Q. Cai, R. Liang, D. Zhang, X. Liu, M. Zhang, Y. Xiong, M. Xu, Q. Liu, P. Li, et al., Copper homeostasis and copper-induced cell death in the pathogenesis of cardiovascular disease and therapeutic strategies, Cell Death Dis. 14 (2023) 105.
[19] D.J. Cao, J.A. Hill, Copper futures: ceruloplasmin and heart failure, Circ. Res. 114 (2014) 1678–1680.
[20] N. Wang, X. Xu, H. Li, Q. Feng, H. Wang, Y.J. Kang, Atherosclerotic lesion-specific copper delivery suppresses atherosclerosis in high-cholesterol-fed rabbits, Exp. Biol. Med. (Maywood, NJ, U. S.) 246 (2021) 2671–2678.
[21] E.J. Ge, A.I. Bush, A. Casini, P.A. Cobine, J.R. Cross, G.M. DeNicola, Q.P. Dou, K.J. Franz, V.M. Gohil, S. Gupta, et al., Connecting copper and cancer: from transition metal signalling to metalloplasia, Nat. Rev. Cancer 22 (2022) 102–113.
[22] L. Yang, X. Chen, H. Cheng, L. Zhang, Dietary copper intake and risk of stroke in adults: a case-control study based on national health and nutrition examination Survey 2013-2018, Nutrients 14 (2022).

[23] M. Zhang, W. Li, Y. Wang, T. Wang, M. Ma, C. Tian, Association between the change of serum copper and ischemic stroke: a systematic review and meta-analysis, J. Mol. Neurosci. : MN. 70 (2020) 475–480.
[24] C. Iadecola, M.S. Buckwalter, J. Anrather, Immune responses to stroke: mechanisms, modulation, and therapeutic potential, J. Clin. Invest. 130 (2020) 2777–2788.
[25] Y. Ma, S. Yang, Q. He, D. Zhang, J. Chang, The role of immune cells in post-stroke angiogenesis and neuronal remodeling: the known and the unknown, Front. Immunol. 12 (2021) 784098.
[26] T. Barrett, S.E. Wilhite, P. Ledoux, C. Evangelista, I.F. Kim, M. Tomashevsky, K.A. Marshall, K.H. Phillippy, P.M. Sherman, M. Holko, et al., NCBI GEO: archive for functional genomics data sets–update, Nucleic Acids Res. 41 (2013) D991–D995.
[27] B. Stamova, G.C. Jickling, B.P. Ander, X. Zhan, D. Liu, R. Turner, C. Ho, J.C. Khoury, C. Bushnell, A. Pancioli, et al., Gene expression in peripheral immune cells following cardioembolic stroke is sexually dimorphic, PLoS One 9 (2014) e102550.
[28] T.L. Barr, Y. Conley, J. Ding, A. Dillman, S. Warach, A. Singleton, M. Matarin, Genomic biomarkers and cellular pathways of ischemic stroke by RNA gene expression profiling, Neurology 75 (2010) 1009–1014.
[29] W. Zhu, L. Tian, X. Yue, J. Liu, Y. Fu, Y. Yan, LncRNA expression profiling of ischemic stroke during the transition from the acute to subacute stage, Front. Neurol. 10 (2019) 36.
[30] N. Zhou, J. Bao, FerrDb: a manually curated resource for regulators and markers of ferroptosis and ferroptosis-disease associations, Database : the journal of biological databases and curation 2020 (2020).
[31] Y. Yuan, M. Fu, N. Li, M. Ye, Identification of immune infiltration and cuproptosis-related subgroups in Crohn's disease, Front. Immunol. 13 (2022) 1074271.
[32] B. Chen, X. Zhou, L. Yang, H. Zhou, M. Meng, L. Zhang, J. Li, A Cuproptosis Activation Scoring model predicts neoplasm-immunity interactions and personalized treatments in glioma, Comput. Biol. Med. 148 (2022) 105924.
[33] C. Yang, C. Delcher, E. Shenkman, S. Ranka, Machine learning approaches for predicting high cost high need patient expenditures in health care, Biomed. Eng. Online 17 (2018) 131.
[34] S. Engebretsen, J. Bohlin, Statistical predictions with glmnet, Clin. Epigenet. 11 (2019) 123.
[35] N.A. Obuchowski, J.A. Bullen, Receiver operating characteristic (ROC) curves: review of methods with applications in diagnostic medicine, Phys. Med. Biol. 63 (2018) 07tr01.
[36] A.M. Newman, C.L. Liu, M.R. Green, A.J. Gentles, W. Feng, Y. Xu, C.D. Hoang, M. Diehn, A.A. Alizadeh, Robust enumeration of cell subsets from tissue expression profiles, Nat. Methods 12 (2015) 453–457.
[37] T. Kakati, D.K. Bhattacharyya, P. Barah, J.K. Kalita, Comparison of methods for differential Co-expression analysis for disease biomarker prediction, Comput. Biol. Med. 113 (2019) 103380.
[38] S. Hänzelmann, R. Castelo, J. Guinney, GSVA: gene set variation analysis for microarray and RNA-seq data, BMC Bioinf. 14 (2013) 7.
[39] T. Wu, E. Hu, S. Xu, M. Chen, P. Guo, Z. Dai, T. Feng, L. Zhou, W. Tang, L. Zhan, et al., clusterProfiler 4.0: a universal enrichment tool for interpreting omics data, Innovation 2 (2021) 100141.
[40] K. Zheng, L. Lin, W. Jiang, L. Chen, X. Zhang, Q. Zhang, Y. Ren, J. Hao, Single-cell RNA-seq reveals the transcriptional landscape in ischemic stroke, J Cereb Blood Flow Metab 42 (2022) 56–73.
[41] D. Aran, A.P. Looney, L. Liu, E. Wu, V. Fong, A. Hsu, S. Chak, R.P. Naikawadi, P.J. Wolters, A.R. Abate, et al., Reference-based analysis of lung single-cell sequencing reveals a transitional profibrotic macrophage, Nat. Immunol. 20 (2019) 163–172.
[42] M. Haupt, S.T. Gerner, M. Bähr, T.R. Doeppner, Neuroprotective strategies for ischemic stroke-future perspectives, Int. J. Mol. Sci. 24 (2023).
[43] D. Nikolic, M. Jankovic, B. Petrovic, I. Novakovic, Genetic aspects of inflammation and immune response in stroke, Int. J. Mol. Sci. 21 (2020).
[44] M. Lai, D. Wang, Z. Lin, Y. Zhang, Small molecule copper and its relative metabolites in serum of cerebral ischemic stroke patients, J. Stroke Cerebrovasc. Dis. 25 (2016) 214–219.
[45] F. Qiu, Y. Wu, A. Zhang, G. Xie, H. Cao, M. Du, H. Jiang, S. Li, M. Ding, Changes of coagulation function and risk of stroke in patients with COVID-19, Brain Behav 11 (2021) e02185.
[46] M.A. Russo, L. Sansone, I. Carnevale, F. Limana, A. Runci, L. Polletta, G.A. Perrone, E. De Santis, M. Tafani, One special question to start with: can HIF/NFkB be a target in inflammation? Endocr. Metab. Immune Disord. - Drug Targets 15 (2015) 171–185.
[47] L. Zhang, W. Wei, X. Ai, E. Kilic, D.M. Hermann, V. Venkataramani, M. Bähr, T.R. Doeppner, Extracellular vesicles from hypoxia-preconditioned microglia promote angiogenesis and repress apoptosis in stroke mice via the TGF-β/Smad2/3 pathway, Cell Death Dis. 12 (2021) 1068.
[48] T.V. Arumugam, S.H. Baik, P. Balaganapathy, C.G. Sobey, M.P. Mattson, D.G. Jo, Notch signaling and neuronal death in stroke, Prog Neurobiol 165–167 (2018) 103–116.
[49] I. Perez-de-Puig, F. Miró-Mur, M. Ferrer-Ferrer, E. Gelpi, J. Pedragosa, C. Justicia, X. Urra, A. Chamorro, A.M. Planas, Neutrophil recruitment to the brain in mouse and human ischemic stroke, Acta Neuropathol. 129 (2015) 239–257.
[50] J. Ruhnau, J. Schulze, A. Dressel, A. Vogelgesang, Thrombosis, neuroinflammation, and poststroke infection: the multifaceted role of neutrophils in stroke, Journal of immunology research 2017 (2017) 5140679.
[51] V. Valsecchi, G. Laudati, O. Cuomo, R. Sirabella, L. Annunziato, G. Pignataro, The hypoxia sensitive metal transcription factor MTF-1 activates NCX1 brain promoter and participates in remote postconditioning neuroprotection in stroke, Cell Death Dis. 12 (2021) 423.
[52] H. Yuan, X. Li, X. Zhang, R. Kang, D. Tang, CISD1 inhibits ferroptosis by protection against mitochondrial lipid peroxidation, Biochemical and biophysical research communications 478 (2016) 838–844.
[53] I.F. Duarte, J. Caio, M.F. Moedas, L.A. Rodrigues, A.P. Leandro, I.A. Rivera, M.F.B. Silva, Dihydrolipoamide dehydrogenase, pyruvate oxidation, and acetylation-dependent mechanisms intersecting drug iatrogenesis, Cell. Mol. Life Sci. : CMLS 78 (2021) 7451–7468.
[54] P. Xiao, J. Gu, W. Xu, X. Niu, J. Zhang, J. Li, Y. Chen, Z. Pei, J. Zeng, S. Xing, RTN4/Nogo-A-S1PR2 negatively regulates angiogenesis and secondary neural repair through enhancing vascular autophagy in the thalamus after cerebral cortical infarction, Autophagy 18 (2022) 2711–2730.
[55] G. Song, H. Dong, D. Ma, H. Wang, X. Ren, Y. Qu, H. Wu, J. Zhu, W. Song, Y. Meng, et al., Tetrahedral framework nucleic acid delivered RNA therapeutics significantly attenuate pancreatic cancer progression via inhibition of CTR1-dependent copper absorption, ACS Appl. Mater. Interfaces 13 (2021) 46334–46342.
[56] M. Arciello, A. Longo, C. Viscomi, C. Capo, A. Angeloni, L. Rossi, C. Balsano, Core domain mutant Y220C of p53 protein has a key role in copper homeostasis in case of free fatty acids overload, Biometals 28 (2015) 1017–1029.
[57] M. Farina, L.E. Vieira, B. Buttari, E. Profumo, L. Saso, The Nrf2 pathway in ischemic stroke: a review, Molecules 26 (2021).
[58] Z.B. Tong, J. Braisted, P.H. Chu, D. Gerhold, The MT1G gene in LUHMES neurons is a sensitive biomarker of neurotoxicity, Neurotox. Res. 38 (2020) 967–978.
[59] L.M. Guthrie, S. Soma, S. Yuan, A. Silva, M. Zulkifli, T.C. Snavely, H.F. Greene, E. Nunez, B. Lynch, C. De Ville, et al., Elesclomol alleviates Menkes pathology and mortality by escorting Cu to cuproenzymes in mice, Science 368 (2020) 620–625.
[60] U. Sehar, P. Rawat, A.P. Reddy, J. Kopel, P.H. Reddy, Amyloid beta in aging and alzheimer's disease, Int. J. Mol. Sci. 23 (2022).
[61] S. Shribman, A. Poujois, O. Bandmann, A. Czlonkowska, T.T. Warner, Wilson's disease: update on pathogenesis, biomarkers and treatments, J. Neurol. Neurosurg. Psychiatry 92 (2021) 1053–1061.
[62] M. Dogan, K. Teralı, R. Eroz, H. Demirci, K. Kocabay, Clinical and molecular findings in a Turkish family with an ultra-rare condition, ELP2-related neurodevelopmental disorder, Mol. Biol. Rep. 48 (2021) 701–708.
[63] F. Azedi, M. Mehrpour, S. Talebi, A. Zendedel, S. Kazemnejad, K. Mousavizadeh, C. Beyer, A.H. Zarnani, M.T. Joghataei, Melatonin regulates neuroinflammation ischemic stroke damage through interactions with microglia in reperfusion phase, Brain Res. 1723 (2019) 146401.
[64] Y. Wang, L. Zhang, F. Zhou, Cuproptosis: a new form of programmed cell death, Cell. Mol. Immunol. 19 (2022) 867–868.
[65] M. Zusso, V. Lunardi, D. Franceschini, A. Pagetta, R. Lo, S. Stifani, A.C. Frigo, P. Giusti, S. Moro, Ciprofloxacin and levofloxacin attenuate microglia inflammatory response via TLR4/NF-kB pathway, J. Neuroinflammation 16 (2019) 148.

[66] L. Luo, M. Liu, Y. Fan, J. Zhang, L. Liu, Y. Li, Q. Zhang, H. Xie, C. Jiang, J. Wu, et al., Intermittent theta-burst stimulation improves motor function by inhibiting neuronal pyroptosis and regulating microglial polarization via TLR4/NFκB/NLRP3 signaling pathway in cerebral ischemic mice, J. Neuroinflammation 19 (2022) 141.
[67] S. Song, L. Yu, M.N. Hasan, S.S. Paruchuri, S.J. Mullett, M.L.G. Sullivan, V.M. Fiesler, C.B. Young, D.B. Stolz, S.G. Wendell, D. Sun, Elevated microglial oxidative phosphorylation and phagocytosis stimulate post-stroke brain remodeling and cognitive function recovery in mice, Commun. Biol. 5 (2022) 35.
[68] Y. Yao, NR4A1 destabilizes TNF mRNA in microglia and modulates stroke outcomes, PLoS Biol. 21 (2023) e3002226.